Int. J. Heat Mass Transfer. Vol. 26, No. 8, pp. 1241–1253, 1983
Printed in Great Britain

0017-9310/83 $3.00 + 0.00
Pergamon Press Ltd.

SOLUTE POLARIZATION DURING PLANAR FREEZING OF AQUEOUS SALT SOLUTIONS

CH. KÖRBER, M. W. SCHEIWE and K. WOLLHÖVER
Helmholtz-Institut für Biomedizinische Technik an der RWTH Aachen, Goethestr. 27/29, D-5100 Aachen, Federal Republic of Germany

(*Received* 18 *May* 1982)

Abstract—An analysis of solute redistribution in binary aqueous salt solutions during unidirectional freezing with a planar solid–liquid interface is presented. A cryomicroscope was equipped with a specially designed freezing stage yielding a well-defined temperature distribution and interface propagation kinetics similar to large systems of plate-like geometry. A microscope spectrophotometer was attached for concentration measurements by means of transmitted light. Aqueous solutions of $NaMnO_4$, exhibiting a maximum absorption at 525 nm and having a phase diagram, as well as mass diffusion properties, very similar to NaCl in water, were used as sample solutions. A major advantage of the method is the combination of quantitative measurements and observation allowing a visual control of the shape of the ice front, and hence of the transition from planar freezing to higher structures. Photometric scans of concentration profiles were recorded during one-dimensional freezing with interface propagation rates between 1 and 10 $\mu m\ s^{-1}$. It was shown that the 'steepness' of the concentration distributions increased with both time and growth velocity. During the initial transient, the results agree well with a mathematical model describing pure mass diffusion at constant ice front velocity. Instabilities of the planar interface resulting in dendritic breakdown always occurred before eutectic or steady-state conditions were reached.

NOMENCLATURE

B	cooling rate [K min^{-1}]
c	concentration [mole fraction or wt %]
D	mass diffusion coefficient [$cm^2\ s^{-1}$]
E	activation energy [J mol^{-1}]
F	area of thermal contact [m^2]
k	thermal conductivity [W $m^{-1}\ K^{-1}$]
k^*	distribution coefficient
P	electrical heating power input [W]
R	universal gas constant [J $mol^{-1}\ K^{-1}$]
t	time [s]
T	temperature [K]
V	heated glass volume [m^3]
x	space coordinate (measured from the plane of symmetry of the freezing stage) [mm]
x'	space coordinate in frame of reference fixed to interface [mm]

Greek symbols

α	heat transfer coefficient [W $m^{-2}\ K^{-1}$]
ξ	interface position [mm]
$\dot{\xi}$	interface velocity [$\mu m\ s^{-1}$]

Subscripts

Cu	copper surface
F	freezing
eut	eutectical
0	initial
r	reference value
R	edge of slit

1. INTRODUCTION

HEAT and mass diffusion problems with a moving boundary separating two regions of different properties play an important role in many physical, chemical, biological and engineering problems. Some important examples are melting and solidification, penetration of liquids into polymers, oxygen absorption in biological tissue, or filtration processes and transport across membranes. The complexity of such problems is mainly due to the conditions prevailing at the moving interface, for instance the liberation or consumption of latent heat, or the rejection or incorporation of certain species. In many situations, the position of the advancing interface is not known *a priori* but is determined by the heat and mass transport mechanisms and properties of the surrounding materials. The literature concerning such problems is extensive—reviews and surveys can be found in refs. [1–8].

The background and motivation for the investigation presented here is the freezing process in biological cell suspensions for cryopreservation purposes, but the results may also be of interest for related metallurgical problems involving alloy properties, crystal pulling and solidification processing.

In biological suspensions, crystallization is generally initiated in the extracellular medium surrounding the biological cells [9–11]. Ice formation in the suspending solution always induces changes in the composition of the residual liquid. The cells exposed to these altered conditions are particularly sensitive to the increasing electrolyte concentration which may eventually become lethal [12]. These conditions and the osmotic reaction of the cells have been analyzed in detail for many cases under the assumption of extracellular equilibrium [10, 13–15]. For incomplete diffusion within the suspension medium, however, such investigations have not yet been published. This lack seems to be due to the difficulties arising when the required liquid and solid temperature and concen-

tration distributions in space and time are to be established. Although numerous theoretical approaches to such coupled problems have been presented [2, 16–21], the results cannot be directly applied to the situation considered here. In most of these cases, simplifying assumptions had to be introduced to enable the problem to be treated mathematically, thus restricting the applicability to situations which may not occur in practice.

Experimental studies, on the other hand, are comparatively rare, probably because of the difficulties associated with the investigation of both heat and mass diffusion in systems undergoing a phase transition and simultaneous control and analysis of interface morphology and propagation kinetics. As far as we know, concentration profiles in freezing salt solutions have been measured in very few studies up to now [22–25]. Unfortunately, these studies did not analyze the structures and instabilities of the advancing ice–liquid interface, presumably because the experimental set-up in combination with the methods applied (conductometry, interferometry, and radioactive tracers) was not suitable. In view of the governing role of the interface morphology with respect to the solute rejection mechanism, the value of the results obtained with these methods appears to be rather limited. It also seems dubious to apply 1-dim. models to a possibly multi-dimensional problem. On the other hand, a number of authors did control or analyze the shape of the solidification front and also the transitions between the various morphologies. Those who performed dynamic measurements [26–29] only employed pure substances, however, and did not investigate solute rejection and chemical interface instabilities.

The aim of this study was to establish a combined experimental technique filling the gap between analyses of solute redistribution during freezing without precise control of the interface morphology and the reverse case. It seemed appropriate at first to limit this study to binary aqueous salt solutions and the solidification of only one component, namely ice. These limitations are not too rigorous to affect any application to biological cells, since many types of cells can be suspended in so-called physiological saline (0.56 mol% NaCl in H_2O) without causing irreversible damage, as lethal concentrations [12] are far below the eutectic point. Generally, two different types of ice formation can be distinguished: planar or 1-dim. freezing with a plane solidification front on one hand, and on the other hand cellular and dendritic crystal growth with needle-shaped or tree-like structures ('dendrites'). Both types of solidification require different experimental (and, of course, theoretical) approaches. This contribution deals with plane front freezing only. Interface instabilities and non-planar crystallization are treated elsewhere [30].

2. EXPERIMENTAL SET-UP

The experimental technique used here essentially evolved from the so-called cryomicroscope [31–33], i.e. a light microscope equipped with a freezing stage allowing controlled cooling and warming as well as simultaneous visual observation of the sample. The most important advantage as compared to other experimental approaches [22–25], is that this method ensures permanent control of the interface morphology, which is of fundamental importance to the process as outlined above. In order to measure concentration profiles, however, additional experimental methods had to be combined with the cryomicroscope. There are a number of possibilities for measuring salt concentrations with high spatial resolution, e.g. interferometry [22, 23] or conductometry [24]. The quantities to be measured, i.e. index of refraction or electrical conductivity, vary with both temperature and concentration in salt solutions. The discrimination necessary to determine the distribution of one quantity from the other imposes considerable problems [22–24]. It was, therefore, considered preferable to measure a different quantity related to concentration, namely light absorption, and therefore a spectrophotometer was combined with the cryomicroscope. The major advantages of this method are that it allows visual observation and control, and the low sensitivity of light absorption to changes in temperature under the conditions studied. (Within the range of temperatures applied, the influence was below the resolution of the system [31].) Furthermore, it allows spatial resolution down to several μm, a fast response sufficient for on-line measurements, and the adaption of position and geometry of the measuring volume to the requirements of each individual experiment.

Material properties

The material of interest to cryobiological applications, sodium chloride in aqueous solution, does not exhibit absorption bands within the visible range of the spectrum. Hence, NaCl had to be replaced by a model substance with an absorptive capacity strong enough for photometric measurements in the thin layers (of some 10 μm) required for light microscopy. Additionally, the mass diffusion properties and the course of the liquidus curve were to be as much as possible the same as in the NaCl–H_2O system. It was found that sodium permanganate ($NaMnO_4$) meets these requirements quite well [31]. As can be seen from Table 1, the diffusion coefficients of both substances are practically equal, as is their temperature dependence according to the relation [31, 34]

$$D(T) = D_r \exp\left[-\frac{E}{R}\left(\frac{1}{T}-\frac{1}{T_r}\right)\right]. \qquad (1)$$

Since the eutectic points are also quite close to each other [35], $NaMnO_4$ represents an excellent model substance to be used instead of NaCl (Table 1). The absorption spectrum in aqueous solution exhibits a maximum at 525 nm with further absorption bands at 506, 545 and 565 nm [31]. Checks of the pro-

Table 1

Quantity	Unit	$NaCl-H_2O$	$NaMnO_4-H_2O$	Ref.
C_{eut}	mole fraction	0.158	0.152	[35]
T_{eut}	K	251.95	257.35	[35]
D_r	10^{-5} cm^2 s^{-1}	0.72	0.69	[31, 34]
E	kJ mol^{-1}	19.70	20.83	[31, 34]

portionality of $NaMnO_4$ concentration and extinction according to the Lambert–Beer law showed that all conditions examined here were well within the linear range [31, 34].

Freezing stage

In order to investigate the desired diffusion and crystallization phenomena, a special freezing stage was developed. Particular attention had to be paid to the control of temperature gradients within the system because of their dominant role in deciding the shape of the solid–liquid interface. (The temperature gradient at the interface is a basic ingredient of the stability theories [36–43] describing the transitions between different interface morphologies.) The well-defined temperature field necessary for the precise control of the crystallization process represents the major difference between the various types of microscope freezing stages used for cryobiological studies [44–49]. In these systems, temperature gradients were as much as possible suppressed in order to obtain isothermal cooling. This, however, does not represent the conditions of solidification in large samples as used technically, where the presence of considerable temperature gradients can generally not be avoided.

The freezing stage designed for the particular purpose of this investigation basically operates by means of a compensation method and nitrogen cooling. Only a small part of the system immediately adjacent to the sample layer is heated locally while the surrounding is being kept at low temperature, thus serving as a cold reservoir. The system, therefore, has a fast thermal response allowing a precise control of temperature and cooling rates up to several 10^3 K min^{-1} [33]. In this respect, the principle of operation is quite similar to other freezing stages [47, 49].

The arrangement of the essential components of the stage is shown in Fig. 1. It consists of a multi-layer composite glass sheet, serving for heating and temperature measurement, which is in thermal contact with a copper surface permanently cooled and thus withdrawing heat from the sample. The composite heating-measuring unit is based on a quadratical quartz sheet of 16 mm edge length and 160 μm thickness, quite similar to an ordinary glass cover slip as commonly used for microscopy (labelled 5 in Fig. 1). Its top surface is covered by a transparent electrically conductive coating (4) which dissipates electrical energy for heating. It can sustain loads up to 10 W cm^{-2} (with compensatory cooling). The electrical leads (9) are soldered to two parallel strips of additionally deposited gold coating (8), 3 mm wide and 10 mm apart. The area in between is insulated electrically by another layer consisting of SiO_2. On top of that, a thermocouple (6), made from 5 μm foils of copper and constantan, is fixed in a layer of about 10 μm epoxy cement covered by a 60 μm glass sheet (3). The sample is placed on the surface of the latter which protects the junction of the thermocouple from mechanical, chemical, and electrical influences and facilitates sample changes and handling. A conventional glass cover slip (1) measuring about 12 × 8 × 0.15 mm is placed on top of the sample

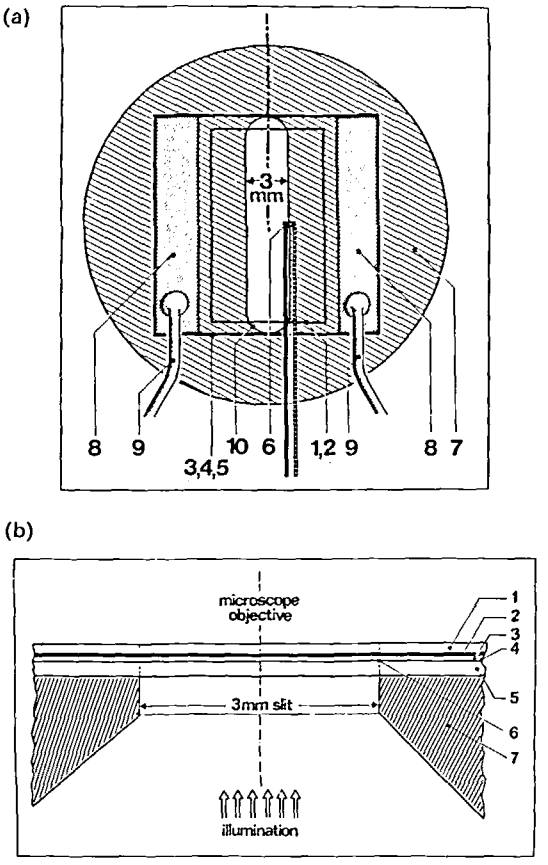

FIG. 1. Top view (a) and cross-sectional drawing (b) of the center part of the freezing stage. 1: 150 μm glass cover slip. 2: 10 μm sample solution layer. 3: 60 μm glass sheet for electrical insulation. 4: electrically conductive coating serving as resistance heater, covered by a coating of silicon dioxide. 5: 160 μm quartz substrate (16 × 16 mm). 6: position of the thermocouple junction (copper–constantan). 7: cooled copper block. 8: gold-coated contact surfaces. 9: electrical leads. 10: edge of slit representing the field of observation.

droplet (about 1 μl) to obtain a layer of about 10 μm thickness (2).

The whole heating–measuring element is placed on a copper block kept at low temperature and serving as a cold reservoir. In order to establish good thermal contact, the element is pressed against the polished copper surface (7) by means of two silicone holders (not shown in Fig. 1). The junction of the thermocouple (6) is located directly above the edge of the slit (10) illuminated from below. The slit, representing the field of observation, causes an inhomogeneity in the otherwise isothermal temperature distribution in the sample layer since heat is not removed by the copper surface in the area above the slit. Freezing is therefore initiated outside that area and starts to advance towards the center of the slit if the electrical power input used for compensatory heating is reduced. Hence the freezing behavior of the system is similar to that of large plate-shaped containers cooled at the outer surfaces [50, 51]. The temperature field will be described and analyzed in detail below. The copper block is surrounded by a helical pipe containing the coolant. It is mounted in a sheet of low thermal conductivity laminated fabric which is fixed to the traversing stage of the microscope.

Microscope system

Observation and analyses were made in transmitted light with a LEITZ-Orthoplan microscope. As shown in Fig. 2, the microscope was equipped with various attachments which will be described briefly in the following.

Microscope photometer. A specially designed spectrophotometer (LEITZ-MPV compact) was combined with the microscope for absorption measurements. The photometer head basically contains the photomultiplier and a mirror system serving to project the photometer diaphragm into the primary image plane. This allows a precise adjustment and selection of the photometric field, i.e. the area to be measured. The spectral sensitivity of the photocathode ranges from about 220 to 750 nm showing a maximum at 420 nm according to the supplier's information. The photometer head was placed on a split-body tube device having a straight tube for measurement and oblique tubes for (simultaneous) viewing. High voltage power was supplied from a control panel also serving for dark current compensation, synchronization of the measuring procedure and digital display of the absorption signal voltage. In order to obtain the desired quantity

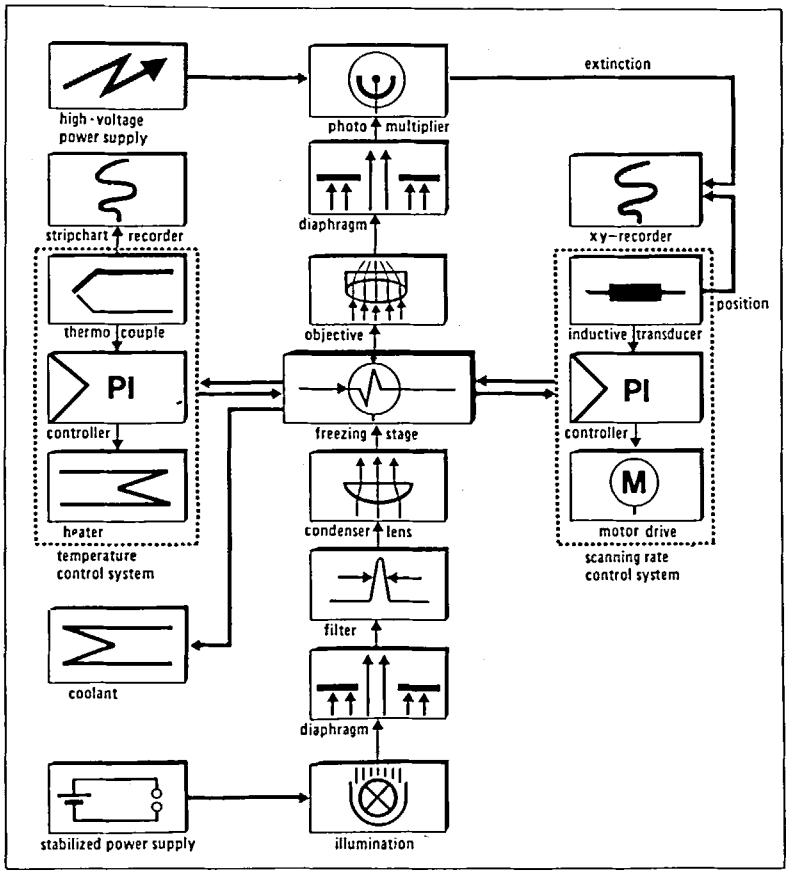

FIG. 2. Schematical representation of the interaction of the components of the experimental set-up.

proportional to concentration, namely extinction, the analogue signal was converted logarithmically and shown on the ordinate of an xy-recorder.

Imaging optics. The specimen was viewed and analyzed with dry objectives of long working distance having magnification factors of 2.5×, 4×, or 32×. For the determination of the total magnification factor, the tube lens (1.25×) and the ocular lens (10×) have to be taken into account. A special head could be used for the additional projection of temperature display and time base signal into the ray path of the microscope.

Illuminating optics and light source. An adjustable rectangular diaphragm corresponding to that within the photometer head can be focussed within the object plane by means of a condenser lens and serves to adjust the luminous field (according to the area to be measured). An interference strip filter with a linear dispersion of 0.42 mm nm^{-1} and a bandwidth of 15 nm was used to select the desired wavelength of 525 nm. The system was illuminated by a 100 W halogen lamp with a stabilized power supply.

Temperature control system. A specially designed feedback control system based on a PI-controller was employed to achieve a wide variety of constant cooling rates and starting temperatures. A detailed description may be found elsewhere [52]. Pre-cooled nitrogen was used to maintain the desired temperature of the copper block. The flow rate was controlled by means of a simple rotameter and adjusted manually. The temperature was displayed digitally and recorded on a strip-chart recorder in order to document the temperature–time history of the freezing process.

Scanning stage. The traversing stage of the microscope was equipped with a DC precision motor drive. The stage could thus be moved transversally across the slit in order to scan the concentration profiles developing across the slit. Scanning rates could be controlled between 150 and 1350 $\mu m\ s^{-1}$ with an accuracy of better than 1.5%. An inductive transducer (dispersion 0.24 V mm^{-1}) served to monitor the position of the measuring beam within the system (representing the x-axis of the recording).

The whole cryomicroscope assembly was placed in a Plexiglass housing with a dry nitrogen gas atmosphere to suppress the condensation of water vapor within the ray path of the optical system.

Experimental procedure

All concentration profiles were recorded with solutions of an initial $NaMnO_4$ content of 0.56 mol% (2.16 wt%) corresponding to physiological saline with an NaCl content of 0.56 mol% (0.9 wt%). The thickness of the solution layer was adjusted by means of the volume of the sample droplet (1 μl) yielding about 10 μm with a cover glass of $8 \times 13\ mm^2$. Under these conditions, the extinction values measured were proportional to concentration up to about ten times the initial salt concentration. The extinction of ice (being equal to that of pure liquid water under the experimental conditions applied here) was used as a reference value. Using an objective of 32× magnification, the size of the (quadratical) photometric field, and hence spatial resolution, was adjusted to 13 μm edge length. The selected scanning velocity of 150 $\mu m\ s^{-1}$ represents a compromise concerning resolution and distortion of the profiles (cf. next section).

Two major problems had to be coped with when carrying out the experiments. First, the penetration of air bubbles into the field of measurement could not always be avoided. Under such circumstances, the experiment was interrupted and repeated. Second, the initial concentration distribution had to be as homogeneous as possible in order to allow comparisons with theoretical results to be made. The difficulty consisted of generating a planar ice front within the field of observation without causing a pronounced concentration profile in front of it. For this reason, the sample was initially frozen with a large supercooling of 15–20 K, giving a fine-grained crystalline structure to the complete sample solution. Subsequently, the sample was warmed slowly by applying the compensatory heating and hence generating the desired temperature distribution across the slit of the freezing stage (cf. next section, Fig. 5). This procedure brought the ice fronts close to the edges of the slit with sufficiently rapid equilibration by solute diffusion within the small domains of segregation. However, as supercooling and, consequently, the structure obtained during freezing is a random process to a certain degree, the initial concentration profiles were not always suitable for quantitative evaluation.

Having obtained starting conditions as desired, electronically controlled cooling rates were generated while the sample was scanned continuously in the manner described above. The temperature of the copper block was kept at −60°C. After dendritic breakdown of the planar interface the recording of profiles was stopped since the orientation of the scanning section to the developing structures could no longer be influenced or predicted.

3. RESULTS AND DISCUSSION

A typical solidification process as observed under the cryomicroscope is illustrated in Fig. 3. The cooling rate was $B = -6.3\ K\ min^{-1}$. Each strip represents the same section of the slit. (The edges are visible at $x = \pm x_R = \pm 1.5$ mm, cf. also Fig. 1.) The temperatures, measured above the edge of the slit, are indicated on each picture. It may be noted that the intervals in temperature, and hence also time, are non-uniform in this example. The freezing process was started at 272 K with an approximately homogeneous solute distribution in the liquid between the ice fronts, located close to the edges at that moment. A slight deviation in the symmetry of

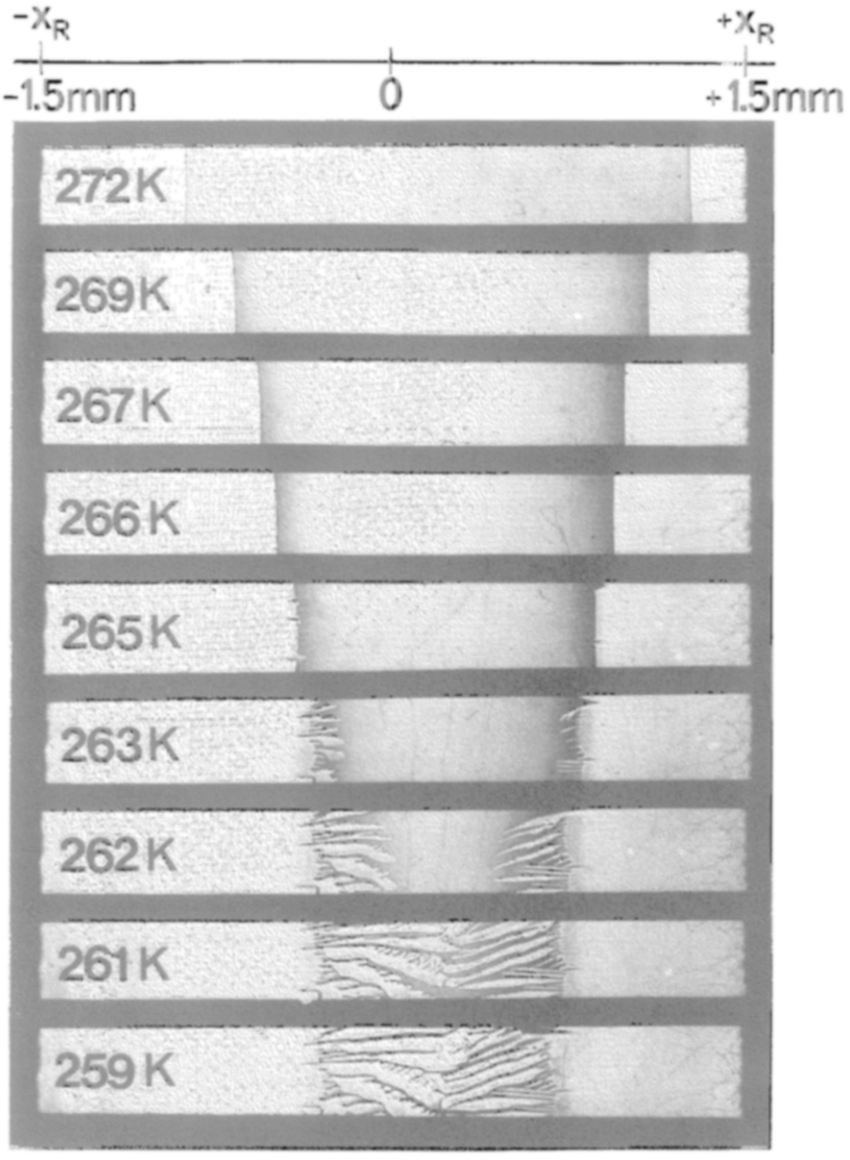

FIG. 3. Sequence of micro-photographs showing the solidification process as observed under the cryomicroscope. The pictures were taken (with non-uniform time intervals) at the temperatures indicated at the left (measured above the edge of the slit). The cooling rate was $B = -6.3\,\mathrm{K\,min^{-1}}$. Each strip represents the same section of the slit with the edges visible at $x = \pm x_R = \pm 1.5$ mm (cf. Fig. 1). From ref. [30].

the temperature distribution resulted from an imperfectly balanced thermal contact between the glass element and the copper surface. As the temperature decreases, both interfaces advance towards the center. Since the solute cannot be incorporated, it is being repelled and redistributed by diffusion. The boundary layer of enriched solute built-up in front of the interface is indicated by the more intense blackening. It can be seen that the ice front remained planar down to 266 K, i.e. for about 60 s with the enriched solute layer becoming more and more pronounced. At 266 K, small grooves can be detected. The next picture (265 K) already shows the formation of needle-shaped ice crystals protruding from those grooves into the residual liquid, and hence entrapping the solute-rich layer. Side-branching and dendritic structures can be recognized after further reduction of the temperature, while the liquid becomes more and more concentrated in the channel-like interstices between the dendritic arms. In the following only the initial phase of planar growth will be considered. Cellular and dendritic freezing are treated elsewhere [30] as mentioned above.

Interface propagation kinetics and temperature field

The interface propagation kinetics for various cases of 1-dim. freezing are summarized in Fig. 4. The diagram shows the time dependence of the interface position ξ measured from the edge of the slit towards the center and determined from the photometric scans

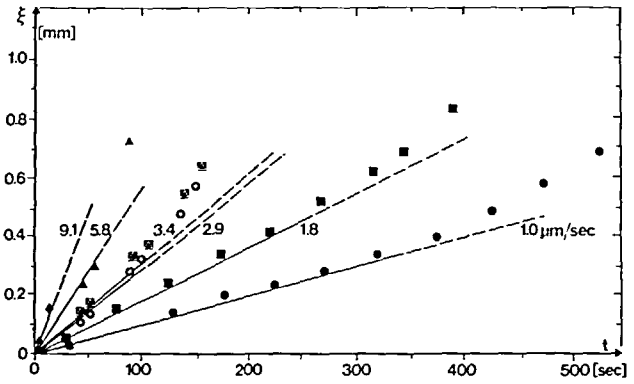

FIG. 4. Propagation of the interface position ξ with time for various cooling rates. The initial ranges were approximated linearly with the initial interface velocities $\dot{\xi}_0$ indicated in $\mu m\ s^{-1}$.

discussed below. In all examples, the temperature (measured by the thermocouple located above the edge of the slit) was lowered linearly with time, i.e. with a constant cooling rate. It can be seen that the motion of the interface becomes accelerated towards the center under these conditions, as indicated in Fig. 4. The initial ranges of the propagation curves can be approximated linearly. The obtained initial interface velocities $\dot{\xi}_0$ of 1.0, 1.8, 2.9, 3.4, 5.8, and 9.1 $\mu m\ s^{-1}$ correspond to cooling rates B of -1.2, -3.1, -6.2, -7.8, -11.9, and $-32\ K\ min^{-1}$, respectively.

The kind of interface motion observed suggests the application of the following simple model [31] to describe the temperature distribution within the field of observation. The model is 1-dim. and neglects thermal effects of the sample layer which is very thin as compared to the surrounding glass elements. The region above the slit is modelled as an infinite solid bounded by two parallel planes at $x = \pm x_R$ which are kept at constant temperature T_R. The resistance heater is regarded as a continuous source distributed homogeneously within the system and generating heat at a constant rate P per unit time and volume V. The steady state solution to the pure conduction problem may be obtained in analogy to the cylindrical system analyzed in [53],

$$T(x) = T_R + \frac{P}{2kV}(x_R^2 - x^2) \qquad (2)$$

where k denotes the thermal conductivity. Furthermore, it is assumed that the power input for the resistance heater is proportional to the temperature difference between the copper block (T_{Cu}) and the edges (T_R),

$$P = \alpha F(T_R - T_{Cu}). \qquad (3)$$

α and F denote the heat transfer coefficient and the thermal contact area, respectively. For the system under consideration, the validity of this relationship was confirmed experimentally [31]. Finally, the temperature at the edges will be lowered at a rate B which is kept constant by the electronical control system,

$$T_R = T_0 + Bt. \qquad (4)$$

Under quasi-stationary conditions, i.e. assuming a sufficiently quick re-establishment of a steady state profile (2) after each change in temperature according to equation (4), one obtains a parabolical temperature distribution,

$$T(x,t) = T_0 + Bt + \frac{\alpha F}{2kV}(T_0 + Bt - T_{Cu})(x_R^2 - x^2). \qquad (5)$$

Figure 5 schematically represents this field with the time t shown as a parameter. It can be seen that the parabolic profile becomes flatter as the temperature is lowered by reducing the electrical power input. The propagation of a certain isotherm, e.g. that of the freezing temperature T_F, is hence also quadratical with time, becoming accelerated towards the center as indicated in Fig. 5. This behavior was checked experimentally with pure water for many cases described in more detail elsewhere [31]. The model was well confirmed for small cooling rates up to some 10 $K\ min^{-1}$ as long as the interface remained flat. (The procedure implies, however, that the ice front is always at its equilibrium freezing temperature. As supercooling at the interface is below 0.1 K for propagation velocities up to about 10 $\mu m\ s^{-1}$ [51], this limitation does not seem to be relevant under the conditions studied here.)

Concentration profiles

Figure 6 shows a space-time representation of the concentration profiles measured during a relatively slow freezing process ($B = -1.2\ K\ min^{-1}$). In this case, the initial interface velocity $\dot{\xi}_0 = 1.0\ \mu m\ s^{-1}$ is very small as well. Under such conditions the ice front remains stable for quite a long time. Dendritic breakdown, apparent from the dentated shape of the last profile recorded, does not occur until both interfaces have almost met in the middle. (The deviation from symmetry mentioned above also appears, of course, on the photometric scans.) Concentration polarization is relatively small in that case because the solute can diffuse away almost as fast as the interface advances. It can be recognized that the concentration of both interfaces increases with time up to 2.3 and 3.1-fold

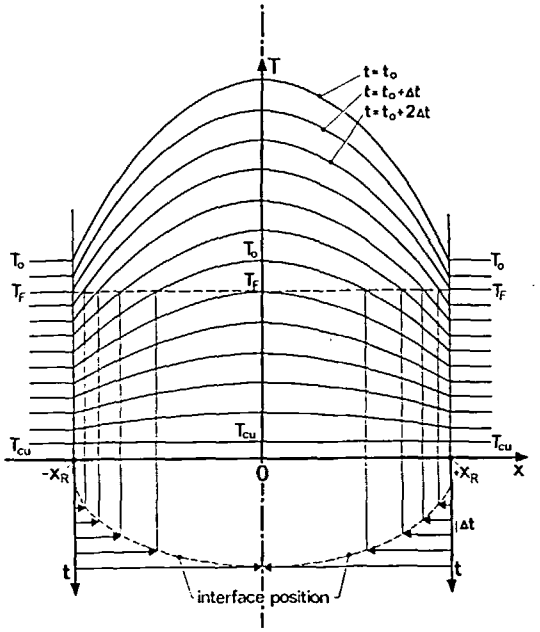

FIG. 5. Schematical parametric representation of the temperature field across the slit and interface propagation according to the model described in the text. T_0, T_F, and T_{Cu} denote the initial, freezing, and copper block temperatures, respectively.

their initial values, respectively. The increase of the minimum concentration between the ice fronts is somewhat larger, namely 3.8-fold. This indicates strong interference between the profiles as they approach each other, becoming significant after about 90 s. (The typical diffusion length, $l = 2D/\xi_0$, is about 1.4 mm and hence very close to the half-length of the system.) It may also be noted that the concentration gradient at the interface increases as well. This behavior is closely related to the stability of the planar ice front which is treated in detail elsewhere [30]. Further quantitative analyses were not performed with the example shown in Fig. 6 because of the relatively non-uniform shape of the initial profile.

Some more examples which were suitable for comparison with theoretical results are presented in Figs. 7–9. The concentration profiles are superimposed as measured with the absorption due to the edges of the slit at $x = \pm 1.5$ mm being visible in Figs. 7 and 8. The profiles were recorded under the conditions indicated in the captions; the initial interface velocities can be derived from the propagation kinetics plotted in Fig. 4. It should be noted that cooling and hence interface motion becomes more and more rapid from Fig. 7 (1.8 μm s^{-1}) to Figs. 8 (2.9 μm s^{-1}) and 9 (9.1, 5.8, 3.4 μm s^{-1}). Dendritic breakdown becomes more and more likely—consequently, the number of planar profiles that could be recorded decreased. (Figure 7 still contains the first 'dendritic' profile which was omitted in Figs. 8 and 9 for clarity.) The small structures superimposed on some of the profiles are due to dust and other impurities in the solution. Those in the solid part of the system result from the fine-grained structure obtained initially (see Section 2). As already mentioned, the initial concentration was $c_0 = 0.56$ mol % (2.16 wt %) $NaMnO_4$ in all cases.

Qualitatively, the following observations may be derived from the experiments:

(1) The concentration at the interface is increasing continuously during the whole freezing process. For this reason, theoretical models considering interface concentrations constant in time [2, 54, 55] cannot be correlated with the results obtained here.

(2) The profiles become 'steeper' as freezing goes on,

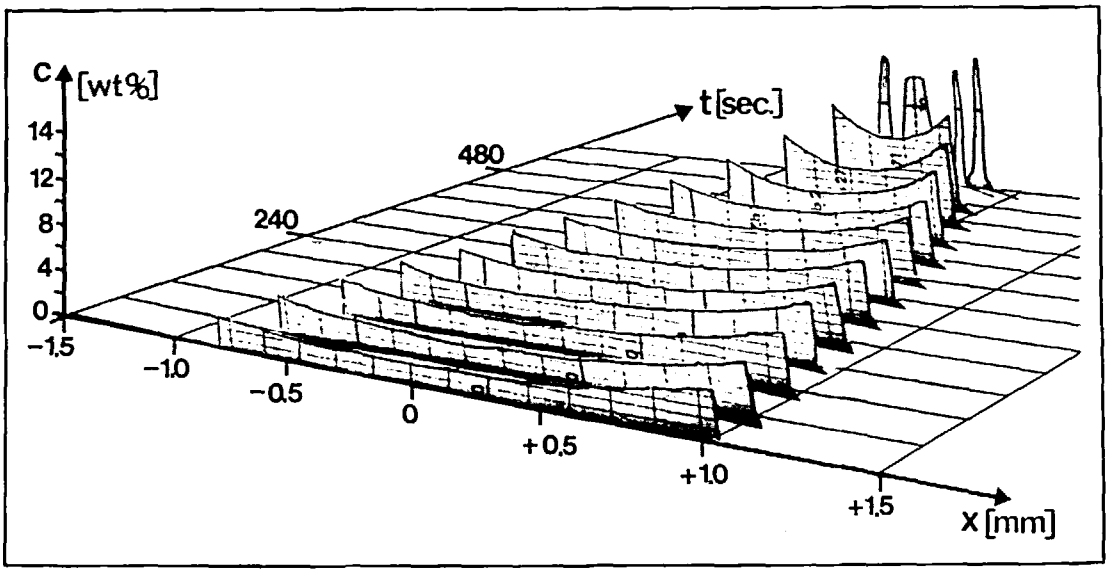

FIG. 6. Space–time representation of measured concentration profiles. Cooling rate $B = -1.2$ K min^{-1}, initial interface velocity $\xi_0 = 1.0$ μm s^{-1}.

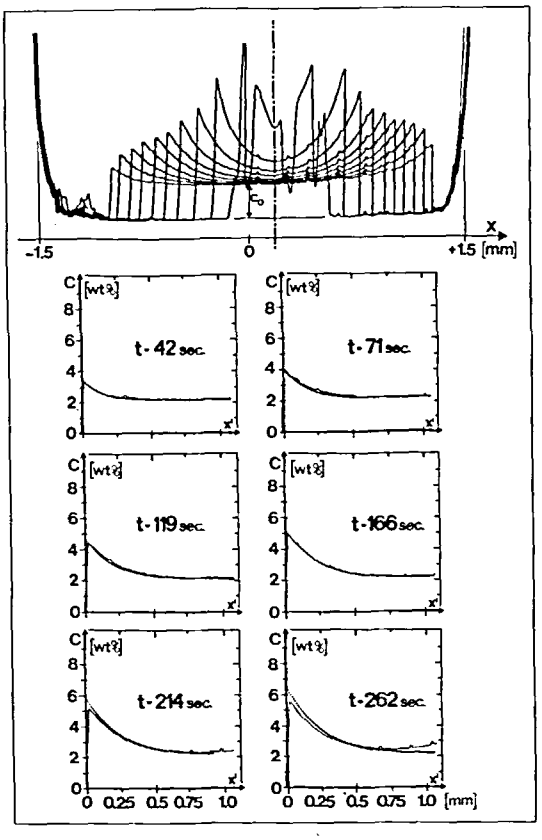

FIG. 7. Superimposed concentration profiles and comparison to theoretical results [dotted curves, equation (10)]. Cooling rate $B = -3.1$ K min^{-1}, initial interface velocity $\dot{\xi}_0 = 1.8$ μm s^{-1}, initial concentration 2.16 wt % $NaMnO_4$.

i.e. the concentration gradients at the interface are increasing as well. The steady state conditions treated by some authors [56, 57] are hence not encountered under the conditions considered here.

(3) In all cases of planar freezing investigated here, the eutectic concentration of 15.2 mol % (41.4 wt %) $NaMnO_4$ is not reached at any point. The precipitation of a second solid component besides ice is therefore not taken into account.

(4) An increase of the minimum concentration between the ice fronts, i.e. interference of the profiles approaching each other, can only be observed for the relatively slow processes with initial interface velocities of less than 2 μm s^{-1} (Figs. 6 and 7). More rapid cooling results in interface breakdown before interference can occur. A semi-infinite model may hence be sufficient to describe the more rapid cooling processes and possibly also the initial transient during slow freezing.

Concentration profiles with properties similar to those mentioned above can be obtained from a mass diffusion model for the solidification of a semi-infinite binary alloy with constant interface velocity [57]. Aqueous solutions can be treated very much in the same way. The essential difference is the non-vanishing solubility of the solute in the solid phase of alloys, resulting in an incorporation of solute molecules at the advancing interface which is usually described by means of a partition coefficient k^*. Aqueous salt solutions, on the other hand, show an almost complete rejection of the solute, with $k^* < 10^{-8}$ [58]. In the following, we shall therefore consider pure mass diffusion during solidification of a binary aqueous solution with $k^* = 0$ and conditions appropriately modified as compared to the case of a binary alloy [57].

The velocity of the interface is assumed to be constant,

$$\dot{\xi} = \dot{\xi}_0 = \text{const.}$$

After a variable transformation from the laboratory system to a frame of reference fixed to the moving interface,

$$x = x' - \dot{\xi} t \tag{6}$$

(x' is measured away from the interface), Fick's second law can be rewritten as

$$D \frac{\partial^2 c}{\partial x'^2} + \dot{\xi} \frac{\partial c}{\partial x'} = \frac{\partial c}{\partial t}. \tag{7}$$

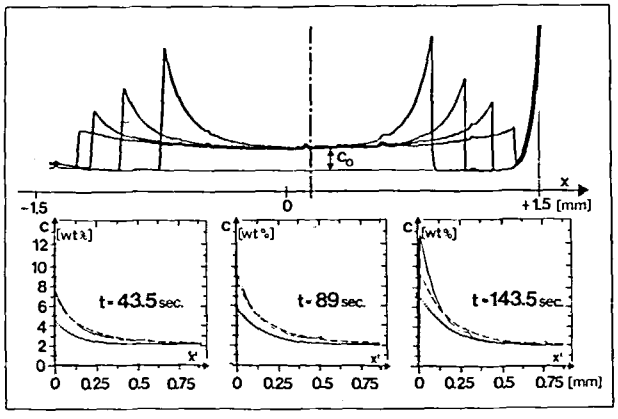

FIG. 8. Superimposed concentration profiles and comparison to theoretical results [dotted curves, equation (10); since the RHS was evaluated, the profiles in the frames are mirror-inverted]. Cooling rate $B = -6.2$ K min^{-1}, initial interface velocity $\dot{\xi}_0 = 2.9$ μm s^{-1}, initial concentration $c_0 = 2.16$ wt % $NaMnO_4$.

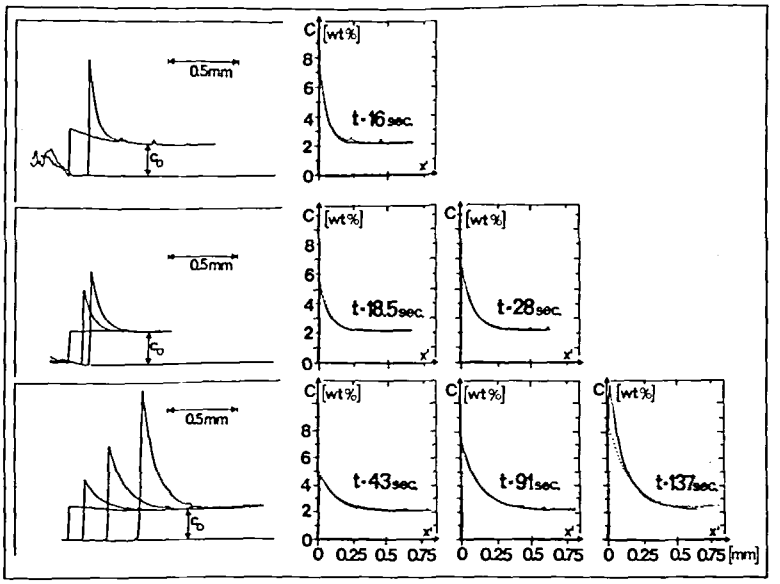

FIG. 9. Superimposed concentration profiles and comparison to theoretical results [dotted curves, equation (10)]. Top: cooling rate $B = -32$ K min^{-1}, initial interface velocity $\xi_0 = 9.1\ \mu$m s^{-1}. Middle: $B = -11.9$ K min^{-1}, $\xi_0 = 5.8\ \mu$m s^{-1}. Bottom: $B = -7.8$ K min^{-1}, $\xi_0 = 3.4\ \mu$m s^{-1}. Initial concentration $c_0 = 2.16$ wt% $NaMnO_4$ in all cases.

The solute concentration is denoted by c, with $c = 0$ in the solid ($x' < 0$) and $c = c(x', t)$ in the liquid ($x' \geqslant 0$). Mass conservation at the interface yields

$$D\frac{\partial c}{\partial x'}\bigg|_0 + \dot{\xi} c|_0 = 0, \quad \text{at } x' = 0, \tag{8}$$

which is sometimes referred to as the "total particle rejection condition" [19]. For a semi-infinite system with a uniform concentration distribution at the beginning, the initial and boundary conditions are

$$c = c_0 \quad \text{at } t = 0 \quad \text{for all } x' \geqslant 0, \tag{9a}$$

$$c = c_0 \quad \text{for } t > 0 \quad \text{and } x' \to \infty. \tag{9b}$$

It is important to mention that the mass diffusion problem described by the equations given above includes neither effects due to convection nor the differences in density between solid and liquid and implies constant material properties.

The solution to equation (7) with conditions (8) and (9) can be obtained in analogy to [57] by use of a Laplace transformation and is derived in detail in ref. [31]. As a result, we shall just present the equation giving the concentration distribution in front of the advancing interface,

$$c(x', t) = c_0\left\{1 + \frac{\dot{\xi} t}{(\pi D t)^{1/2}} \exp\left[-\left(\frac{x' + \dot{\xi} t}{2(Dt)^{1/2}}\right)^2\right] + \frac{1}{2}\left[1 - \frac{\dot{\xi}}{D}(x' - \dot{\xi} t)\right] e^{-(\dot{\xi}/D)x'} \operatorname{erfc}\left(\frac{x' - \dot{\xi} t}{2(Dt)^{1/2}}\right) - \frac{1}{2}\operatorname{erfc}\left(\frac{x' + \dot{\xi} t}{2(Dt)^{1/2}}\right)\right\}. \tag{10}$$

The concentration profiles computed from the above equation may be compared with the experimental results, particularly during the initial part of the freezing process when the interface velocity is approximately constant and if the initial distribution is about homogeneous. In the evaluation of equation (10), a rational approximation for the error function (erf) with an accuracy of better than 1.5×10^{-7} [59] was used. The numerical values for $\dot{\xi}$ and c_0 which were put into equation (10) were those indicated in the captions to Figs. 7–9 with the initial interface velocities determined as mentioned above. The diffusion coefficient D was taken at 0°C according to equation (1), i.e. $D = 0.69 \times 10^{-5}$ cm^2 s^{-1}. The spatial distributions $c(x')$ shown in Figs. 7–9 (dotted lines) were computed at times t as indicated for the individual profiles in the frames, with t determined at the moment when the scanning beam was at the interface position.

The comparison between theory and experiment shows very good agreement and almost identical profiles for the more rapid freezing experiments shown in Fig. 9, where the initial distributions are nearly uniform and interference does not occur because of the early breakdown of the planar ice front. Only the last profile recorded ($t = 137$ s) for $\dot{\xi} = 3.4\ \mu$m (lower right in Fig. 9) is steeper than calculated. This discrepancy is probably caused by the increasing velocity of the interface deviating from linearity markedly at that time according to Fig. 4. It may also be noted that the measured profiles are not perfectly vertical at $x' = 0$ because of the limited resolution of the system in space and time, i.e. the finite size of the photometric field (13 μm) and the non-ideal response of the photometer and recorder. A distortion of the profiles predicted theoretically from the non-instantaneous scanning

mode, which is expected to be larger in size for the more rapid cooling experiments, cannot be detected in Fig. 9 and hence may be neglected here.

The family of profiles shown in Fig. 7 did not at first agree equally well as those in Fig. 9 with the results calculated from equation (10). The deviation is largely due to the inhomogeneity of the starting distribution generated by the first freezing with a large degree of supercooling as outlined in Section 2. In the case shown in Fig. 7, the initial distribution ($t = 0$) is, however, congruent to the profile calculated for $t = 42$ s (upper left in Fig. 7). Hence, the non-uniform initial profile may be taken into account by an 'anteponement' of the starting time, i.e. adding a time interval of $t = 42$ s to the actual time of the experiment. (This method of correction is applied frequently in diffusion experiments [60, 61].) This procedure yields quite a good agreement between computed and measured profiles up to about 200 s. The profile at the lower right of Fig. 7 ($t = 262$ s) already exhibits a visible deviation from calculation for $x' \gtrsim 0.6$ mm. At that moment, the profiles are about 1.6 mm apart from each other and start to interfere ($l = 0.8$ mm).

The example shown in Fig. 8 also exhibits a non-uniform initial distribution. The correction method applied above, however, did not succeed in that case as the calculated profiles were always 'steeper' than the initial distribution. Again, it may be worthwhile to recall that the shape of the initial profile could not be perfectly controlled, hence different types of correction may be appropriate from case to case. The desired uniform distribution ($c = c_0$ for $x' \geqslant 0$) was first subtracted from the measured initial profile. That difference, representing the deviation from homogeneity, was then superimposed on the calculated (dotted) curves by addition, resulting in the dashed profiles in Fig. 8. These agree reasonably well with those measured up to about 90 s. Afterwards, the profiles become steeper again due to the accelerated motion of the interface (cf. Fig. 4).

4. SUMMARY AND CONCLUSIONS

The mechanism of solute rejection during freezing of a binary aqueous salt solution in a finite system has been analyzed experimentally. A well-defined temperature field was established in order to control the motion and shape of the advancing ice–liquid interface. Under these conditions, the spatial distribution of solute during the freezing process was measured at fixed intervals in time for a variety of interface propagation rates. Observation of the interface morphology revealed that dendritic breakdown of the initially planar ice front always occurred before eutectic or steady state conditions were reached. During the period of the initial transient, when the interface propagation rate was approximately constant, concentration profiles calculated from a pure mass diffusion model agreed well with those measured photometrically.

While heat and mass transfer during freezing are generally fully coupled [16–21, 51], the experimental set-up employed here allowed a separate and independent treatment and analysis of solute redistribution. Such an uncoupling of the problem is possible because the temperature field within the sample is mainly determined by the surrounding glass sheets used for fixation and hence is independent of the sample properties itself, whose thermal effects can be neglected. In this respect, the experimental results cannot be directly transferred to situations of unidirectional freezing in large plate-shaped containers as used for practical purposes where the freezing behavior is substantially affected by the sample solution.

In two important points, however, the design of the experimental set-up is such that it does exhibit principal similarities to the freezing process as it occurs in extended containers. First, the thermal gradient in the liquid region, and, hence, its stabilizing effect against deformations of the planar ice front, decreases continuously from the edges (outer surfaces) towards the center; second, the motion of the interfaces becomes accelerated towards the center if a temperature decrease linear with time is imposed at the edges (surfaces). Both effects can also be derived from a numerical solution of the fully coupled 1-dim. problem [51]. The resulting concentration distributions also show the same tendency as observed here, i.e. an increasing 'steepness' of the profiles with both time and interface velocity. Our results hence underline the usefulness of cryomicroscopy as a powerful means for real-time analysis of solidification phenomena in general and also its relevance to 'practical' freezing situations.

Acknowledgements—The partial support of this study by the 'Studienstiftung des Deutschen Volkes' is gratefully acknowledged. The authors would also like to thank Professor J. Schnakenberg (Inst. f. Theoret. Physik der RWTH Aachen) for his continuing advice and helpful discussions during the course of this research.

REFERENCES

1. T. R. Ockendon and R. W. Hodgkins, *Moving Boundary Problems in Heat Flow and Diffusion*. Clarendon Press, Oxford (1975).
2. L. I. Rubinstein, The Stefan problem, *Trans. Math. Monogr.* **27**, 52–59 (1971).
3. R. L. Parker, Crystal growth mechanisms: energetics, kinetics, and transport, in *Solid State Physics*, Vol. 25 (edited by H. Ehrenreich, F. Seitz and D. Turnbull). Academic Press, New York (1970).
4. H. S. Peiser, *Crystal Growth*. Pergamon Press, Oxford (1967).
5. S. G. Bankoff, Heat conduction or diffusion with change of phase, in *Advances in Chemical Engineering*, Vol. 5 (edited by T. B. Drew, J. W. Hoopes and T. Vermuelen). Academic Press, New York (1964).
6. J. C. Muehlbauer and J. E. Sunderland, Heat conduction with freezing or melting, *Appl. Mech. Rev.* **18**, 951–959 (1965).
7. B. R. Pamplin. *Crystal Growth*, Pergamon Press, Oxford (1975).
8. D. G. Wilson, A. D. Solomon and P. T. Boggs. *Moving Boundary Problems*, Academic Press, New York (1978).

9. H. Molisch, *Untersuchungen über das Erfrieren von Pflanzen*. Verl. G. Fischer, Jena (1897).
10. P. Mazur, Kinetics of water loss from cells at subzero temperatures and the likelihood of intracellular freezing, *J. Gen. Physiol.* **47**, 347–369 (1963).
11. P. Mazur, The role of intracellular freezing in the death of cells cooled at supraoptimal rates, *Cryobiology* **14**, 251–272 (1977).
12. J. E. Lovelock, The hemolysis of human red blood cells by freezing and thawing, *Biochim. Biophys. Acta* **10**, 414–426 (1953).
13. O. M. Silvares, E. G. Cravalho, W. M. Toscano and C. E. Huggins, The thermodynamics of water transport from biological cells during freezing, *Trans. Am. Soc. Mech. Engrs*, Series C, *J. Heat Transfer* **97**, 582–588 (1975).
14. G. A. Mansoori, Kinetics of water loss from cells at subzero centigrade temperatures, *Cryobiology* **12**, 34–45 (1975).
15. G. R. Ling and C. L. Tien, Analysis of cell freezing and dehydration: Fundamental studies of cell freezing and dehydration, ASME paper 69 WA/HT 31 (1969).
16. J. Tsubaki and B. H. Boley, One-dimensional solidification of binary mixtures, *Mech. Res. Commun.* **4**, 115–122 (1977).
17. R. Levin, The freezing of finite domain aqueous solutions: solute redistribution, *Int. J. Heat Mass Transfer* **24**, 1443–1455 (1981).
18. B. A. Boley, Time dependent solidification of binary mixtures, *Int. J. Heat Mass Transfer* **21**, 821–824 (1978).
19. M. G. O'Callaghan, An analysis of the heat and mass transport during the freezing of biomaterials, Ph.D. Thesis, Mech. Engng., MIT, Cambridge, Mass. (1978).
20. A. B. Tayler, The mathematical formulation of Stefan problems, in *Moving Boundary Problems in Heat Flow and Diffusion* (edited by J. R. Ockendon and W. R. Hodgkins). Clarendon Press, Oxford (1975).
21. K. Rädle, Numerische Lösung der gekoppelten Wärmeleitung und Verdunstung, *Wärme* **85**, 109–111 (1979).
22. B. W. Grange, Diffusion of heat and solute during freezing of salt solutions, Ph.D. Thesis, Mech. Engng., Purdue University, Indiana (1975).
23. B. W. Grange, R. Viskanta and H. Stevenson, Diffusion of heat and solute during freezing of salt solutions, *Int. J. Heat Mass Transfer* **19**, 373–384 (1976).
24. J. P. Terwilliger and S. F. Dizio, Salt rejection phenomena in the freezing of saline solutions, *Chem. Engng Sci.* **25**, 1331–1349 (1970).
25. G. Kvajić, V. Brajović and E. R. Pounder, Rejection of impurities by growing ice from a melt, in *Physics of Ice* (edited by N. Riehl, B. Bullemer and H. Engelhardt). Plenum, New York (1969).
26. S. C. Hardy and S. R. Coriell, Morphological stability of a growing cylindrical crystal of ice, *J. Appl. Phys.* **39**, 3505–3507 (1968).
27. S. C. Hardy and S. R. Coriell, Morphological stability and the ice-water interfacial free energy, *J. Crystal Growth* **3**, 569–573 (1968).
28. M. E. Glicksman, R. J. Schaefer and J. D. Ayers, Dendritic growth—a test of theory, *Metall. Trans.* **7A**, 1747–1759 (1976).
29. K. A. Jackson and J. D. Hunt, Transparent compounds that freeze like metals, *Acta Met.* **13**, 1212–1215 (1965).
30. C. Körber and M. W. Scheiwe, Observations on the non-planar freezing of aqueous salt solutions, *J. Crystal Growth* **61** (in press).
31. C. Körber, Das Gefrieren wäßriger Lösungen in biologischen Substanzen, Doctoral Dissertation Math.-Naturwiss. Fak., RWTH Aachen (1981).
32. M. W. Scheiwe, Untersuchungen zum Verfahren der Langzeitkouservierung lebender Blukzellen durch Gefrieren. Doctoral Dissertation Fak. Maschinenwesen, RWTH Aachen (1981).
33. M. W. Scheiwe and C. Körber, Thermally defined cryomicroscopy and some applications on human leukocytes, *J. Microscopy* **126**(1), 29–44 (1982).
34. C. Körber, K. Wollhöver and M. W. Scheiwe, The redistribution of solute in front of the advancing ice–liquid interface, *Refrigeration Science and Technology*, pp. 161–170. IIR Documentary Series, Paris (1981).
35. Landolt-Börnstein, *Zahlenwerte und Funktionen*. II. Band 2b. Springer, Berlin (1962).
36. J. W. Rutter and B. Chalmers, A prismatic substructure formed during solidification of metals, *Can. J. Phys.* **31**, 15–39 (1953).
37. W. W. Mullins and R. F. Sekerka, Stability of the planar interface during solidification of a dilute binary alloy, *J. Appl. Phys.* **35**, 444–451 (1964).
38. R. F. Sekerka, Application of the time-dependent interface stability to an isothermal phase transformation, *J. Phys. Chem. Solids* **28**, 983–994 (1967).
39. R. F. Sekerka, Morphological stability, *J. Crystal Growth* **3**, 71–81 (1968).
40. R. T. Delves, The theory of the stability of the solid–liquid interface under constitutional supercooling (I), *Phys. Stat. Sol.* **16**, 621–632 (1966).
41. R. T. Delves, The theory of the stability of the solid–liquid interface under constitutional supercooling (II), *Phys. Stat. Sol.* **17**, 119–130 (1966).
42. J. S. Langer, Instabilities and pattern formation in crystal growth, *Rev. Mod. Phys.* **52**, 1–28 (1980).
43. D. J. Wollkind and L. A. Segel, A non-linear stability analysis of the freezing of a diluted binary alloy, *Phil. Trans. R. Soc.* **268A**, 351–380 (1970).
44. A. U. Smith, C. Polge and J. Smiles, Microscopic observation of living cells during freezing and thawing, *Royal Microscop. Soc.* **71**, 186–195 (1951).
45. G. Rapatz and B. Luyet, Microscopic observations on the development of the ice phase in the freezing of blood, *Biodynamica* **8**, 195–239 (1960).
46. T. Nei, Mechanism of hemolysis of erythrocytes by freezing at near-zero temperatures. I. Microscopic observation of hemolysing erythrocytes during the freezing and thawing process, *Cryobiology* **4**, 153–156 (1967).
47. K. R. Diller and E. G. Cravalho, A cryomicroscope for the study of freezing and thawing processes in biological cells, *Cryobiology* **7**, 191–199 (1971).
48. K. C. Gupta, The mechanism of cryohemolysis: by direct observation with the cryomicroscope and the electron microscope, *Cryobiology* **12**, 417–426 (1975).
49. J. J. McGrath, E. G. Cravalho and C. E. Huggins, An experimental comparison of intracellular ice formation and freeze–thaw survival of Hela S-3 cells, *Cryobiology* **12**, 540–550 (1975).
50. T. Geiser and M. W. Scheiwe, Design of freezing containers for submerging into LN_2: the temperature field and its influence on the recovery of hydroxyethyl starch preserved red blood cells, *Cryo-Lett* **2**, 291–300 (1981).
51. C. Körber and M. W. Scheiwe, Unidirectional freezing of binary aqueous solutions: an analysis of transient diffusion of heat and mass (in preparation).
52. P. Schwindke and M. W. Scheiwe, Regeleinheit mit wählbarer Führungsgröße des Frierprozesses für die Gefrierkonservierung biologischer Zellen, *Biomed. Techn.* **23**(suppl.), 87 (1978).
53. H. Gröber, S. Erk and U. Grigull, *Die Grundgesetze der Wärmeübertragung*, p. 121. Springer, Berlin (1963).
54. R. L. Levin, Generalized analytical solution for the freezing of a super-cooled aqueous solution in a finite domain, *Int. J. Heat Mass Transfer* **23**, 951–959 (1980).
55. H. Müller-Krumbhaar, Diffusion theory for crystal growth at arbitrary solute concentration, *J. Chem. Phys.* **63**, 5131–5138 (1975).
56. W. A. Tiller, K. A. Jackson, J. W. Rutter and B. Chalmers, The redistribution of solute atoms during the solidification of metals, *Acta Met.* **1**, 428–437 (1953).

57. V. G. Smith, W. A. Tiller and J. W. Rutter, A mathematical analysis of solute redistribution during freezing, *Can. J. Phys.* **33**, 723–745 (1955).
58. J. D. Harrison and W. A. Tiller, in *Ice and Snow* (edited by W. D. Kingerey) p. 215. MIT Press, Cambridge, Mass. (1963).
59. M. Abramowitz and I. A. Segun, *Handbook of Mathematical Functions*, p. 299. Dover, New York (1968).
60. W. Jost, *Diffusion in Solids, Liquids, Gases*, p. 445. Academic Press, New York (1960).
61. J. Crank, *The Mathematics of Diffusion*, p. 51. Clarendon Press, Oxford (1956).

LA REDISTRIBUTION DU SOLUTE PAR GEL PLANAIRE DES SOLUTIONS SALINES AQUEUSES

Résumé—L'analyse traite de la redistribution d'un soluté dans des solutions salines aqueuses par gel unidirectionnel avec une interface solide–liquide planaire. Pour ce faire fut conçue spécialement une platine de congelation installée dans un cryomicroscope, avec une distribution de la température bien définie et une cinétique du développement de la glace semblables à celles réalisées dans des grands réservoirs en forme de plaque. Les mesures de concentration furent effectuées par transparence avec un microscope-spectrophotomètre. Comme soluté fut utilisé le $NaMnO_4$ qui possède un maximum d'absorption à 525 nm et dont le diagramme de phases et le comportement de diffusion sont très semblables à ceux du NaCl dans l'eau. Un avantage certain de cette méthode d'examen est la combinaison des mesures quantitatives avec l'observation au microscope qui permet un contrôle visuel de la forme du front de glace et par la des passages du gel planaire à des structures plus complexes. Des profils de concentration mesurés photométriquement furent relevés pour des vitesses de l'interface entre 1 et 10 $\mu m\,s^{-1}$. Il fut démontré que l'inclinaison de la répartition de concentration augmente avec le temps et avec la vitesse de croissance. Dans la periode initiale, les résultats correspondent bien avec un modèle mathématique décrivant la pure diffusion de matière à vitesse constante du front de glace. Des instabilités de l'interface planaire avec passage à une congélation dendritique furent toujours observeés avant que des comportements eutectiques ou stationnaires puissent être obtenus.

DIE LÖSUNGSSEGREGATION BEIM PLANAREN GEFRIEREN WÄSSRIGER SALZLÖSUNGEN

Zusammenfassung—Die Untersuchung behandelt die Umverteilung gelöster Substanz in wässrigen Salzlösungen beim eindimensionalen Gefrieren mit planarer Phasengrenze fest-flüssig. Hierfür wurde ein speziell ausgelegter Friertisch mit wohldefinierter Temperaturverteilung und Eisausbreitungskinetik ähnlich wie in großen plattenförmigen Behältern in ein Kryomikroskop eingesetzt. Die Konzentrationsmessungen wurden im Durchlicht mit einem Mikroskop-Spectralphotometer durchgeführt. Als gelöste Substanz wurde $NaMnO_4$ verwendet, das ein Absorptionsmaximum bei 525 nm besitzt und dessen Phasendiagram und Diffusionsverhalten dem von NaCl in Wasser ähnlich ist. Ein wesentlicher Vorteil dieser Untersuchungsmethode ist die Verbindung quantitativer Messungen mit mikroskopischer Beobachtung, die eine visuelle Kontrolle der Gestalt der Eisfront und damit der Übergänge zwischen planarem Gefrieren zu höheren Strukturen ermöglicht. Photometrisch gemessene Konzentrationsprofile wurden für Phasengrenzgeschwindigkeiten zwischen 1 und 10 $\mu m\ s^{-1}$ aufgenommen. Es wurde gezeigt, daß die "Steilheit" der Konzentrationsverteilungen mit der Zeit und der Wachstumsgeschwindigkeit zunimmt. Im anfänglichen Bereich stimmen die Resultate gut mit einem mathematischem Modell für diffusiven Stofftransport bei konstanter Geschwindigkeit der Eisfront überein. Instabilitäten der glatten Phasengrenze mit Übergang zu dendritischer Erstarrung wurden immer beobachtet bevor eutektische oder stationäre Verhältnisse erreicht werden konnten.

ПОЛЯРИЗАЦИЯ РАСТВОРЕННОГО ВЕЩЕСТВА ПРИ ПЛОСКОМ ЗАМОРАЖИВАНИИ ВОДНЫХ СОЛЕВЫХ РАСТВОРОВ

Аннотация—Представлен анализ перераспределения растворенного вещества в бинарных водных солевых растворах при направленном замораживании с плоской границей раздела твердое тело–жидкость. В конструкции криомикроскопа была специально предусмотрена стадия замораживания, которая позволяла получать четкие распределения температуры и определять кинетику продвижения границы раздела аналогично большим системам с геометрией в виде пластины. К микроскопу был подсоединен спектрофотометр для измерения концентрации путем регистрации поглощения пропущенного света. В качестве образцов использовались водные растворы $NaMnO_4$ с максимальным поглощением при 525 нм, фазовая диаграмма и характеристики диффузии массы которых аналогичны растворам NaCl в воде. Основным достоинством метода является сочетание количественных измерений с визуальным наблюдением, позволяющим контролировать форму фронта льда и тем самым переход от плоского фронта замораживания к более сложным структурам. Фотометрическое сканирование профилей концентраций производилось в течение одномерного замораживания при скорости продвижения границы раздела в диапазоне от 1 до 10 $\mu м\ с^{-1}$. Показано, что «крутизна» распределений концентрации увеличивалась с увеличением времени и скорости роста льда. В течение начального переходного режима результаты хорошо согласуются с математической моделью, описывающей чистую диффузию массы при постоянной скорости продвижения фронта льда. До устанавливания эвтектических или стационарных условий постоянно наблюдались неустойчивости плоской границы раздела, приводящие к дендритным прорывам.